Resilience-based seismic risk assessment of aging bridge networks under climate change

L. Capacci & F. Biondini
Department of Civil and Environmental Engineering, Politecnico di Milano, Milan, Italy

ABSTRACT: Risk assessment of transportation networks exposed to seismic hazard should be based on time-variant probabilistic performance indicators taking into account the aging and deterioration of bridges caused by environmental stressors. In this context, climate change may exacerbate the deterioration rate, harming the capacity of the overall network to sustain the impact of earthquakes without experiencing disproportionate loss of functionality due to excessive traffic flow downtime. This paper presents a probabilistic framework for seismic risk assessment of aging transportation systems based on a quantitative measure of network resilience. The proposed framework integrates the traffic response of the transportation system with the time-variant seismic capacity assessment of reinforced concrete structures exposed to chloride-induced corrosion and prescribed climate change scenarios. The results of the application allow quantifying the detrimental impact of climate change to each single vulnerable facility in the road network and, in turn, on the overall transportation lifeline.

1 INTRODUCTION

Life-cycle risk assessment of infrastructure systems and lifelines is crucial for the prosperity of communities in hazard-prone areas. The performance under emergency conditions of vulnerable infrastructure systems exposed to extreme events, such as earthquakes, can be assessed in terms of resilience, i.e. the ability of a system to withstand the effects of disruptive events and to recover promptly and efficiently the pre-event functionality (Bruneau *et al*. 2003, Decò *et al*. 2013, Capacci *et al.* 2020). The social impact of historical seismic events provides a clear example of the increasing need of building resilient transportation networks, in which bridges are frequently the most vulnerable components (Basöz and Kiremidjian 1998).

The seismic capacity and resilience of key bridges within transportation networks can be severely impaired over time by environmental stressors (Biondini *et al.* 2015, Capacci *et al.* 2020). Climate change may also significantly alter the deterioration rate of materials and components exacerbating the effects of aging and structural deterioration of bridges and infrastructure systems (Stewart *et al.* 2011, Mondoro *et al.* 2017, Nasr *et al.* 2019). In this context, optimal life-cycle management strategies of critical road networks should be informed by time-variant performance indicators able to incorporate global warming effects that may affect the long-term resilience of infrastructure systems (Capacci and Biondini 2019).

This paper proposes a probabilistic framework for life-cycle resilience-based seismic risk assessment that integrates the road network traffic response with the time-variant seismic vulnerability assessment of reinforced concrete (RC) bridges exposed to seismic hazard, environmental stressors, and temperature increase under uncertainty. The probabilistic resilience of road networks is defined and quantified based on the capability of essential bridges to sustain over time the effects of sudden disruptive events without suffering damage that would force infrastructure managers to impose prolonged traffic restrictions for the sake of users' safety, harming the functionality of the overall transportation network due to excessive traffic flow downtime.

The proposed risk measure is assembled by three main components: the probabilistic seismic hazard model at the regional scale, the seismic capacity of vulnerable bridges in the network, and the system exposure representing the consequences of bridge seismic damage and deterioration at the infrastructural level. The time-variant mean annual rate of exceedance of resilience target thresholds is assessed based on the probabilistic seismic hazard scenario affecting a road network with aging RC bridges exposed to chloride-induced corrosion under prescribed temperature increase scenarios. The results of the presented application allow quantifying the detrimental impact of climate change effects to each single vulnerable facility in the road network and, in turn, on the overall transportation lifeline.

2 RESILIENCE-BASED RISK ASSESSMENT

2.1 *Seismic hazard scenario*

The first component in risk assessment is associated with the quantification of hazards, namely the set of physical phenomena that can cause structural damage and operational disruption. Probabilistic Seismic Hazard Analysis (i.e. PSHA) aims to describe the occurrence rate of severe seismic events at a specific site of interest based on the characteristics of active tectonic faults in the area of interest (McGuire 2004).

The seismic intensity at any location in the region affected by seismic events is a generally represented as a lognormal random field given the vector of seismic hazard parameters $\mathbf{H}_h$, which collects the n_h basic random variables that allow predicting the rate of occurrence and severity of earthquakes in the region (e.g. moment magnitude, epicenter location, etc). Therefore, the seismic intensity scenario $\mathbf{I}$ is a multivariate random variable representing the seismic intensity at the site of the n_b vulnerable bridges within the network. The parameters of the lognormal random field are conditioned on a set of seismic hazard parameters $\mathbf{H}_h$ based on a suitable ground motion prediction equation (GMPE) accounting for the inter- and intra-event variability of the shaking intensity and the spatial distribution of the bridge sites with respect to the seismic source. The probability density function (PDF) of the seismic intensity scenario $f_\mathbf{I}(\mathbf{i})$ is defined based on total probability theorem as follows:

$$f_\mathbf{I}(\mathbf{i}) = \int_{\Re^{n_h}} f_{\mathbf{I}|\boldsymbol{\eta}_h}(\mathbf{i}|\boldsymbol{\eta}_h) \cdot f_{\mathbf{H}_h}(\boldsymbol{\eta}_h) \cdot d\boldsymbol{\eta}_h \quad (1)$$

where $\mathbf{i}$ and $\boldsymbol{\eta}_h$ are the vectors collecting the outcomes of seismic intensities and hazard parameters.

Based on the common assumption that the occurrence of seismic events of given intensity follows a Poisson process, the differential annual rate of exceedance of a given seismic intensity scenario is defined as follows:

$$|d\lambda(\mathbf{i})| = \left(\sum_{k=1}^{n_f} \nu_k\right) \cdot f_\mathbf{I}(\mathbf{i}) \cdot d\mathbf{i} \quad (2)$$

where ν_k is the annual rate of earthquake occurrence for each of the k-th out of n_f seismogenic sources in the region.

2.2 *Bridge network seismic vulnerability*

The second component of risk assessment consists in the quantification of the system vulnerability, which provides the probability that the network undergoes a specific damage state in the aftermath of a hazardous event. The marginal vulnerability of aging bridges can be assessed based on the exceedance probability of damage state s_b (i.e. fragility curve), corresponding to the time-variant cumulative distribution function (CDF) of the bridge seismic capacity $I_{s,b}$ with respect to the damage state itself:

$$P[S_b(t) \geq s_b|i_b] = F_{I_{s,b}(t)}\big(i_b(t)\big) \quad (3)$$

where S_b is a discrete univariate time-variant random variable representing the damage state of the b-th bridge in the network. The time-dependency in bridge fragility is due to the fact that the vulnerability of each bridge can be affected by detrimental effects of physical damage suffered due to aging effects coupled with extreme loading conditions during the bridge lifetime and the beneficial effects of maintenance and retrofit investments designed to improve the structural reliability (Biondini *et al.* 2006, Marí and Bairán 2008). In the present paper, the dependency with time of bridge seismic capacity is associated with aging and deterioration of the structural system and time-variant fragility curves. Other sources of damage could be incorporated such as the cumulative earthquake damage under successive earthquake shocks (Kumar *et al.* 2009).

Fragility curves represent the exceedance probability of a damage state given i_b at the b-th bridge. The occurrence probability of such damage state corresponds to the difference between fragility curves associated with subsequent damage states as follows:

$$P[S_b(t) = s_b|i_b] = F_{I_{s-1,b}(t)}(i_b) - F_{I_{s,b}(t)}(i_b) \quad (4)$$

The occurrence of a specific bridge damage combination $\mathbf{s}$ given the seismic intensity scenario $\mathbf{i}$ can be defined as the probability of the intersection of the set of events representing the damage state occurrence s_b of each bridge given the seismic intensity i_b at the bridge site:

$$\{\mathbf{S}(t) = \mathbf{s}|\mathbf{i}\} = \left\{\cap_{b=1}^{n_b}[S_b(t) = s_b|i_b]\right\} \quad (5)$$

where $\mathbf{S}$ is a discrete multivariate time-variant random variable representing the combination of bridge damage states. It is worth noting that the occurrence probability of a given damage combination $\mathbf{s}$ does not only depend on the seismic intensity at each site i_b, but also on the correlation between the seismic capacities of each pair of bridges in the network (Capacci and Biondini 2018, Capacci *et al.* 2020).

2.3 *Lifetime seismic risk of bridge networks*

The third component of risk assessment regards the system exposure, which quantifies based on appropriate performance indicators the operational disruption due to earthquake-induced structural damage. After

the occurrence of a seismic event at time t_0, infrastructure managers may be forced to apply a set of traffic limitations due to the damage suffered by the vulnerable bridges in the network. Repair activities allow releasing at discrete time instants t_j the traffic restrictions when the bridge load-carrying capacity is restored. The system functionality profile for a given damage combination **s** can be defined in stepwise form as follows:

$$Q(t;\mathbf{s}) = Q_j(\mathbf{s}) \quad t_j(\mathbf{s}) \le t < t_{j+1}(\mathbf{s}) \tag{6}$$

where n_j is the number of recovery steps and Q_j and t_j are the j-th recovery step functionality level and the time instant, respectively, $\forall j \in [0, n_j(\mathbf{s})]$. In particular, $t_{n+1}=t_h$ corresponds to a prescribed horizon time. The functionality levels Q_j, the recovery time instants t_j and the number of recovery steps n_j are affected by uncertainties related to the recovery strategy adopted for each bridge. In the proposed framework, the recovery process is directly related to the post-earthquake damage state of each bridge collected in vector **s**. Further details on the model for functionality assessment are provided in Capacci *et al.* (2020).

In the proposed framework, the resilience measure is quantified given the occurrence of a bridge damage combination **s** as the integral mean of the functionality profile from the time of occurrence time t_0 up to a fixed horizon time t_h:

$$R(\mathbf{s}) = \frac{1}{\Delta t_h} \int_{t_0}^{t_h} Q(t;\mathbf{s}) dt \tag{7}$$

The uncertainties in the constitutive parameters of the functionality profile are also affecting the resilience measure. Based on the total probability theorem (Ang and Tang 2007), the time-variant CDF of the resilience measure conditional on a given seismic intensity scenario **i** can be defined as the weighted sum of the marginal resilience measure CDFs associated with a prescribed bridge damage combination **s** weighted by its probability of occurrence under given **i** (Capacci and Biondini 2020):

$$F_{R(t)|\mathbf{i}} = \sum_{k=1}^{n_f} F_{R|\mathbf{s}} \cdot P[\mathbf{S}(t) = \mathbf{s}|\mathbf{i}] \tag{8}$$

Given the Poissonian nature of the seismic hazard scenario, seismic risk can be quantified based on the annual failure rate of meeting a prescribed target for the resilience measure as follows:

$$\nu_{R \le r}(r,t) = \int_{\Re_+^{n_b}} F_{R(t)|\mathbf{i}}(r|\mathbf{i}) \cdot |d\lambda(\mathbf{i})| \tag{9}$$

3 PROBABILISTIC DAMAGE ASSESSMENT

3.1 *Corrosion initiation time*

Empirical evidence shows that the complex nature of aggressive agents transport in concrete can be effectively represented as a diffusive process, motivating the adoption of Fick's diffusion model to represent analytically the chloride ingress in concrete (Bertolini *et al.* 2004). The solution of the diffusion equation allows defining the initiation of corrosion damage, triggered at time t_{cr} when the chloride concentration reaches a critical threshold value C_{cr}. The numerical solution of the diffusion equation could be achieved by means of cellular automata (Biondini *et al*. 2004, Titi and Biondini 2016). In the applications of this paper, 2D and 3D diffusion effects are negligible and the solution of the 1D Fick's model is considered (Duracrete 2000, fib 2006, Stewart *et al.* 2011):

$$C(x,t) = C_0 \left[1 - \mathrm{erf}\left(\frac{x}{2\sqrt{f_T(t) \cdot D \cdot t}}\right)\right] \tag{10}$$

where D is the reference diffusivity coefficient, x is the concrete cover depth. The function $f_T(t)$ models the effect of temperature on diffusivity based on Arrhenius Law (Stewart *et al.* 2011):

$$f_T(t) = \exp\left[\frac{E_a}{R_g}\left(\frac{1}{293} - \frac{1}{273+\bar{T}(t)}\right)\right] \tag{11}$$

where E_a=40 kJ/mol is the activation energy of the diffusion process, R_g=8.314×10^{-3} kJ/mol K is the gas constant and $\bar{T}(t)$ is the time-variant average temperature in Celsius degrees. It is worth noting that high temperatures have a detrimental impact on corrosion initiation, reducing the resistivity of concrete to the ingress of aggressive agents.

3.2 *Corrosion penetration rate*

Corrosion leads to a local breakdown of steel protective oxide film in alkaline concrete and acts as anode for the cathodic reaction of oxygen reduction taking place with the surrounding still passive areas. Pits of irregular shape are produced where corrosion takes place with a rate proportional to the electrical current density i_{corr} developed during the chemical reaction (Bertolini *et al.* 2004). Experimental evidence indicates that the corrosion rate increases with temperature and the following stepwise linear relationship is used (Duracrete 2000, Stewart *et al.* 2011, Bastidas-Arteaga *et al.* 2013):

$$i_{corr}(t) = i_{corr-20} \cdot \big(1 + K(T(t) - 20)\big) \tag{12}$$

where $i_{corr\text{-}20}$ is the corrosion rate at 20°C, $T(t)$ is the time-variant temperature profile and K=0.025 or K=0.073 when the temperature is lower or larger than 20 °C, respectively.

Based on Faraday's law, the corrosion current density is proportional to steel mass loss, which can be expressed in terms of the pitting penetration rate:

$$\frac{\partial p_s}{\partial t} = \frac{e_{ech}}{\rho_s} R_f \cdot i_{corr}(t) \quad t \geq t_{cr} \tag{13}$$

where p_s is the corrosion penetration depth and ρ_s is the steel volumetric mass density, $e_{ech}=M/(zF)$ is the electrochemical equivalent of a corroding metal, M=55.8 g/mol is the iron molar mass, F=96493 C/mol is Faraday's constant, z is the ion valence formed following the anodic reaction (generally assumed to be 2). The pitting factor R_f is typically between four and eight (Gonzalez *et al.* 1995) and it defines the ratio between pit penetration depth and average penetration depth measured empirically to calibrate the corrosion rate. The time-variant penetration depth $p_s(t)$ can be evaluated integrating numerically the penetration rate as a function of the temperature profile.

3.3 *Mechanical damage of RC members*

Pitting corrosion leads to a localized loss of steel mass of irregular form generally described by simplified geometrical models, such as hemispherical shapes with radius equal to the penetration depth (Val and Melchers 1997, Biondini and Vergani 2015). The reduction of resisting area of a corroded bar is defined in terms of the time-variant deterioration index δ_s (i.e. percentage mass loss) scaling the undamaged steel bar area A_{s0} as follows:

$$A_s(t) = [1 - \delta_s(t)] \cdot A_{s0} \tag{14}$$

Tensile tests on corroded bars show that limited mass loss may lead reinforcing steel bars to experience brittle failure modes (Almusallam 2001). Experimental evidences also show that the amount of mass loss can be informative of the reduction of steel ductility induced by the corrosion process (Apostolopoulos and Papadakis 2008). Furthermore, the formation of oxidation products leads to the propagation of longitudinal cracks along the concrete cover up to its delamination and spalling. The effects of such degradation process can be modelled by reducing the effective concrete compression strength f_c in terms of the deterioration indices of the steel longitudinal reinforcement bars δ_s. Further details on the degradation laws adopted in this paper for longitudinal reinforcement area, steel ductility, and concrete cover strength are presented in Biondini and Vergani (2015).

3.4 *Probabilistic environmental damage assessment*

The aging process is affected by uncertainties and the time-variant PDF of the bridge deterioration indices $\boldsymbol{\delta}_b(t)$ can be quantified based on the total probability theorem:

$$f_{\boldsymbol{\delta}_b(t)}(\boldsymbol{\delta}_b) = \int_{\Re^{n_e}} f_{\boldsymbol{\delta}_b(t)|\boldsymbol{\eta}_e}(\boldsymbol{\delta}_b|\boldsymbol{\eta}_e) \cdot f_{\mathbf{H}_e}(\boldsymbol{\eta}_e) d\boldsymbol{\eta}_e \tag{15}$$

In particular, $\boldsymbol{\delta}_b(t) \in [0,1]$ is a multivariate stochastic process defining the n_δ bridge deterioration indices with outcomes $\boldsymbol{\delta}$ and the vector $\mathbf{H}_e$ collecting the n_e basic variables that constitute the multivariate distribution of environmental hazard, whilst vectors $\boldsymbol{\eta}_e$ collects their outcomes. It is worth noting that the notation adopted for the environmental hazard assessment is consistent with the one used for seismic hazard assessment.

Therefore, time-variant fragility curves can be defined based on the damage-dependent fragility curves and the total probability theorem:

$$\begin{aligned} F_{I_{s,b}(t)}(i_b) = \int_{[0\times1]^{n_\delta}} \int_{\Re^{n_k}} & F_{I_{s,b}|\boldsymbol{\delta},\boldsymbol{\kappa}}(i_b|\boldsymbol{\delta},\boldsymbol{\kappa}) \cdot \\ & \cdot f_{\boldsymbol{\delta}_b(t)}(\boldsymbol{\delta}) \cdot \\ & \cdot f_{\boldsymbol{\kappa}}(\boldsymbol{\kappa}) d\boldsymbol{\kappa}\, d\boldsymbol{\delta} \end{aligned} \tag{16}$$

where $\mathbf{K}$ and $\boldsymbol{\kappa}$ collect the n_k random variables and their outcomes, respectively constituting the multivariate distribution of basic bridge mechanical parameters.

4 APPLICATION

4.1 *Seismic hazard scenario*

Area sources are often used in practice when the complex spatial distribution of the epicenters of historical earthquakes discourages the choice of hazard models that attribute them to their causative fault (Barani *et al.* 2009). Figure 1 represents the ZS9 seismic zonation related to the Italian scenario. The benchmark network is located in the city of L'Aquila represented by the white dot in Figure 1 (Lat. 42.35°, Lon. 13.40°) surrounded by "zone 923".

The area source is characterized by the normal prevalent faulting mechanism and truncated Gutenberg-Richter distribution (Gutenberg and Richter 1944) presented in Figure 2 (thin line), with shape parameter b=1.05, annual recurrence rate of events with magnitude $\nu_{m\geq4.76}$=0.14, and minimum and maximum moment magnitude $m_{\min}$=4.76 and $m_{\max}$=7.06, respectively (MPS Working Group 2004).

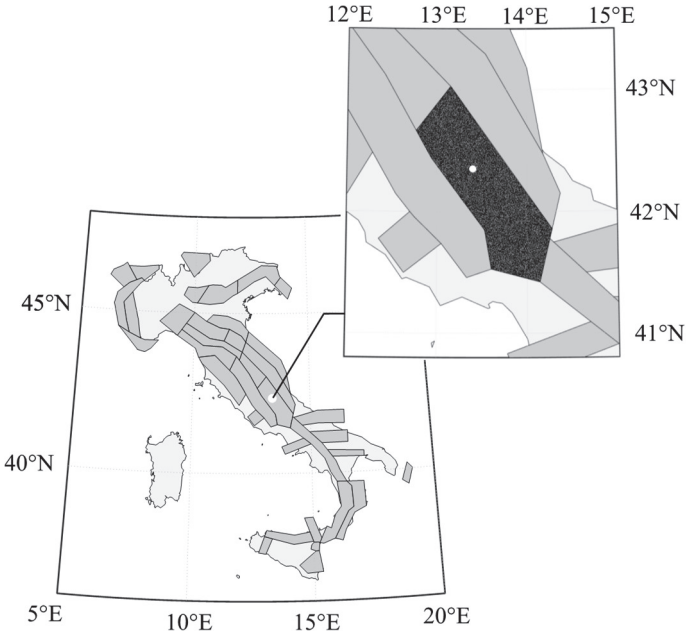

Figure 1. ZS9 seismic zonation and sample epicenter locations at the site of interest.

The ground motion prediction model derived from the Italian strong motion database is adopted (Bindi *et al.* 2011). The prediction model allows simulating the seismic intensity measures i_b at each bridge site given source-to-site distances and moment magnitudes. A simulation framework based on Importance Sampling has been adopted to reduce the computational effort without compromising the accuracy of the risk estimates (Jayaram and Baker 2010). The black dots in Figure 1 represent 2000000 realizations of the sample epicenter locations within the selected are sources. The same number of samples is drawn from the right-skewed distribution represented with thick line in Figure 2, characterized by a probabilistic model of the truncated Gutenberg-Richter distribution with shape parameter b=-1.0. This allows increasing the likelihood of sampling earthquakes leading to higher seismic intensities at the bridge sites and, in turn, severe damage state combinations.

4.2 *Temperature scenarios and aging process*

Two temperature scenarios are considered. The first scenario assumes constant average annual temperature of 15°C and equal annual duration of hot and cold season and peak seasonal temperature variations equal to ±10°C. Seasonal variations are taken into account with sinusoidal oscillations about the average temperature trend (Bastidas-Arteaga *et al.* 2013).

A second scenario under climate change is characterized by a constant increase of the average annual with rate +0.04·°C/year and a linear increase in the annual duration from 50 to 60% for hot season and 50 to 40% for cold season. Figure 3 represents the prescribed temperature profiles with and without climate change (continuous and dashed lines, respectively).

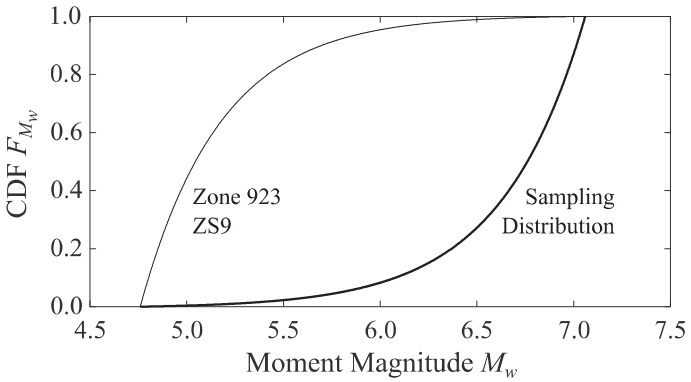

Figure 2. Truncated Gutenberg-Richter CDFs for zone 923 of ZS9 zonation (thin line) and for selected sampling distribution (thick line).

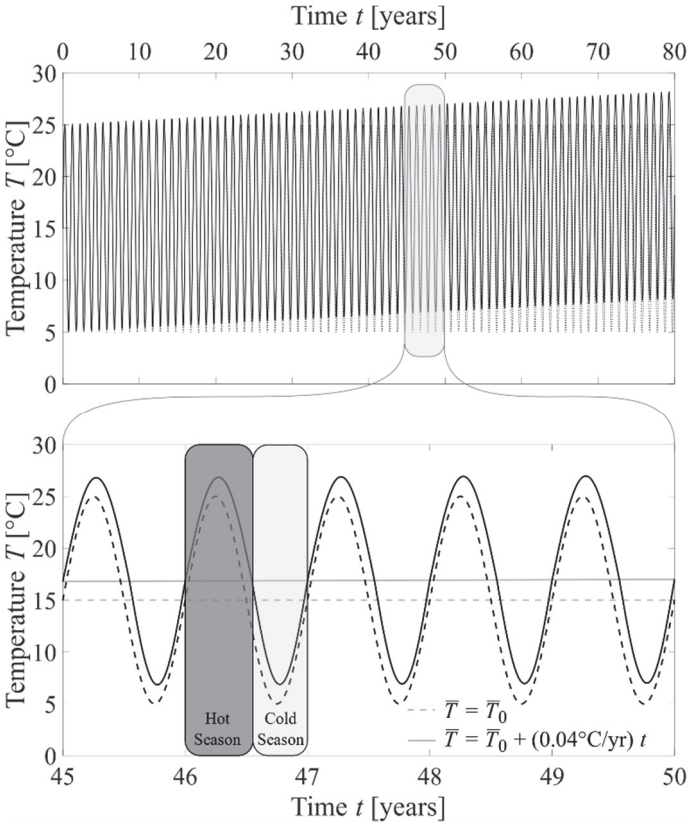

Figure 3. Prescribed temperature scenarios with (continuous line) and without (dashed line) climate change effects.

Table 1. Random variables associated with environmental hazard.

Variable	Distribution	Mean Value μ	C.o.V.
Diffusivity D	Truncated Positive Normal	15.8×10^{-12} m^2/sec	0.20
Aging Coefficient a	Beta between 0.0 and 1.0	0.30	0.12 / μ
Surface Concentration C_0	Truncated Positive Normal	4.0 wt.%/c	0.20
Critical Concentration C_{cr}	Beta between 0.2 and 2.0 wt.%/c	0.6 wt.%/c	0.15 wt.%/c / μ
20°C Corrosion rate $i_{corr,20}$	Lognormal	2.586 μA/cm^2	1.724 μA/cm^2 / μ
Pitting Factor R_f	Gumbel	7.1	0.17 / μ

Monte Carlo simulations are carried out to assess the time-variant probability density function of the deterioration index. Table 1 collects distributions and parameters of the aleatory uncertainties involved in the deterioration process. Figure 4 represents the time-variant empirical CDF of the deterioration index δ_s every 20 years for the prescribed temperature scenarios. Early initiation and rapid rate of corrosion induced by climate change can have a substantial impact on the percentage mass loss of steel bars.

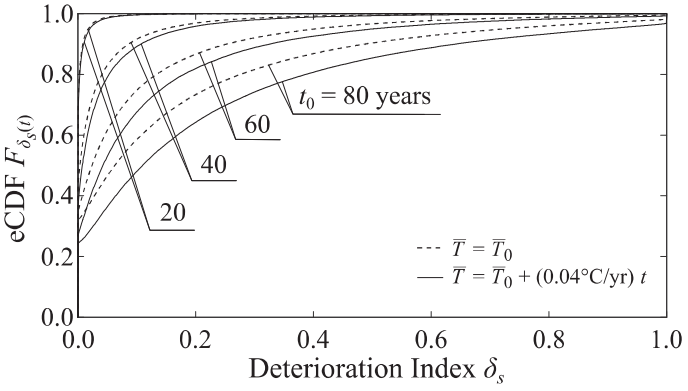

Figure 4. Time-variant empirical CDF of the steel damage index with (continuous lines) and without (dashed lines) temperature increase.

4.3 *Aging fragility curves under climate change*

The three-span continuous RC bridge shown in Figure 5a (adapted from Bouassida *et al.* 2012) is analyzed. The total length of the bridge is 81 m, with lateral spans and central span of 23 and 35 m, respectively. The height of both piers is 8.5 m and, as shown in Figure 5b, they are characterized by circular cross-section reinforced with 21 steel bars with 32mm-diameter. Table 2 collects the basic random variables associated with model uncertainties of the bridge piers: concrete strength f_c, yielding strength f_{sy} and damping ratio ξ (with positive truncated normal distribution). The deck is modeled as elastic system (Capacci *et al.* 2020).

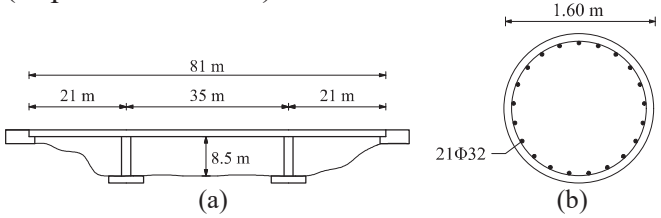

Figure 5. RC bridge. (a) Longitudinal profile; (b) piers cross-section.

Table 2. Random variables associated with bridge properties.

Variable	Mean Value μ	CoV
Concrete Strength f_c	38 MPa	5 MPa / μ
Yielding Strength f_{sy}	500 MPa	30 MPa / μ
Damping Ratio ξ	3.0%	0.4

Damage state exceedance is associated with the attainment of progressively restrictive conditions on a damage measure χ_b, informative of the accumulation of excessive plastic strains in critical regions after the occurrence of a seismic event of intensity i_b. In this paper, χ_b is the maximum response curvature at the base of the bridge piers and the attainment of each damage state is associated with the capacity thresholds $\bar{\chi}_{s,b}$ defined as follows:

- Slight Damage: $\bar{\chi}_{s,b}(s_b = 1) = \chi_{y,b}$
- Moderate Damage: $\bar{\chi}_{s,b}(s_b = 2) = \chi_{y,b} + 0.3\chi_{p,b}$
- Extensive Damage: $\bar{\chi}_{s,b}(s_b = 3) = \chi_{y,b} + 0.6\chi_{p,b}$
- Structural Collapse: $\bar{\chi}_{s,b}(s_b = 4) = \chi_{u,b}$.

In particular, $\chi_{p,b}$=$\chi_{u,b}$-$\chi_{y,b}$ is the margin between ultimate curvature $\chi_{u,b}$ and first yielding curvature $\chi_{y,b}$. The failure probabilities for each intensity measure i_b are computed based on a procedure involving importance sampling on the deterioration damage index δ_s. Fragility curves are then calibrated by linear regression given the failure probability at given intensity measures i_b (Lallemant *et al.* 2015) fitting a lognormal model for seismic capacity:

$$F_{I_{s,b}(t)} = \Phi\left(\frac{\ln i_b - \lambda_{s,b}(t)}{\zeta_{s,b}(t)}\right) \tag{17}$$

where $\lambda_{s,b}$ and $\zeta_{s,b}$ are mean and standard deviation, respectively, of the logarithm of the seismic capacity $I_{s,b}$. Figure 6 shows the time-variant parameters of the fragility curves from 0 to 80 years every 5 years. The thickness of each line increases with damage severity. The seismic vulnerability to first yielding occurrence (s_b=1) is slightly affected by chloride-induced corrosion, whilst aging dramatically reduces the median and increases the dispersion of fragility curves for any damage state s_b>1. The climate change scenario exacerbates such trends, increasing medians decay and dispersions increase rate.

4.4 *Target resilience annual exceedance rate*

The seismic resilience of the simple road network shown in Figure 7 is investigated (Capacci and Biondini 2020). The network includes one Origin node (O) and one Destination node (D) of the traffic demand connected by a main highway with two identical bridges at a relative distance of 5 km. The seismic capacity of the bridge pair is assumed to be statistically independent. The OD pair is also connected by a secondary detour route with a re-entry link. Further details on the adopted model for post-earthquake bridge recovery under uncertainty and the assessment of functionality profile and network resilience are presented in Capacci and Biondini (2018, 2020).

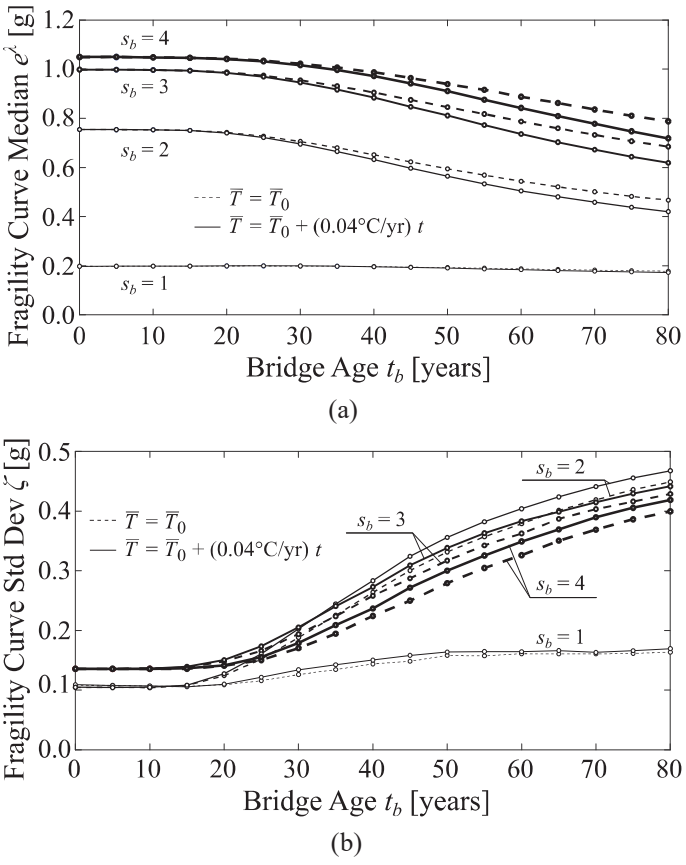

Figure 6. Time-variant parameters of bridge seismic fragility curves: (a) median and (b) logarithmic standard deviation.

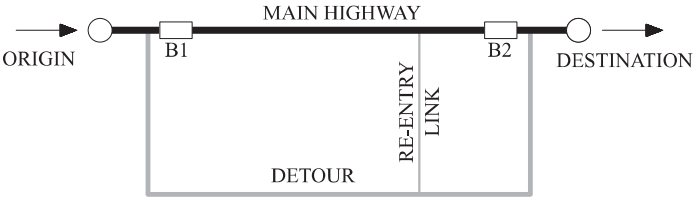

Figure 7 – Benchmark road network with spatially distributed aging RC bridges.

Figure 8 shows in semi-logarithmic scale the numerical estimate of the lifetime annual rate of failure in meeting a prescribed target of network resilience between 80 and 90%. The annual failure risk measure v_r increases with large resilience targets, associated with higher performance levels that the network is required to fulfill. Bridge aging can severely affect the annual failure rate after 20 years, namely when the deterioration process remarkably affects the fragility curves of moderate to severe damage states compared to the pristine bridge conditions, i.e. t_0=0.

Figure 9 represents the annual failure rate in meeting a prescribed resilience target of 85%. These results emphasize the detrimental impact of the climate change scenario. The seismic risk measure under rising temperatures increases of one order of magnitude when the infrastructure reaches 50 years of age, about five years earlier with respect to the scenario with constant average temperature.

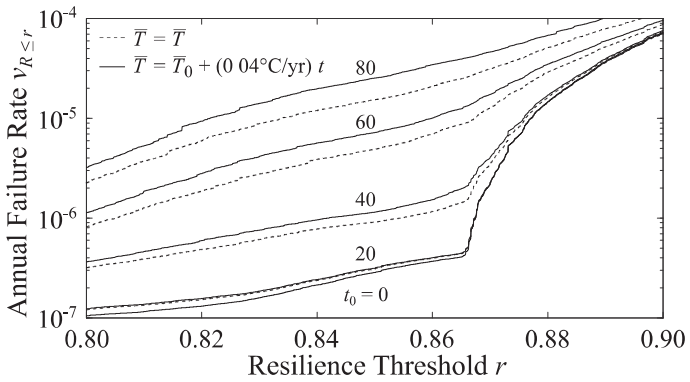

Figure 8. Annual rate of failure in meeting a prescribed target of network resilience between 80 and 90% at different times with (continuous lines) and without (dashed lines) climate change.

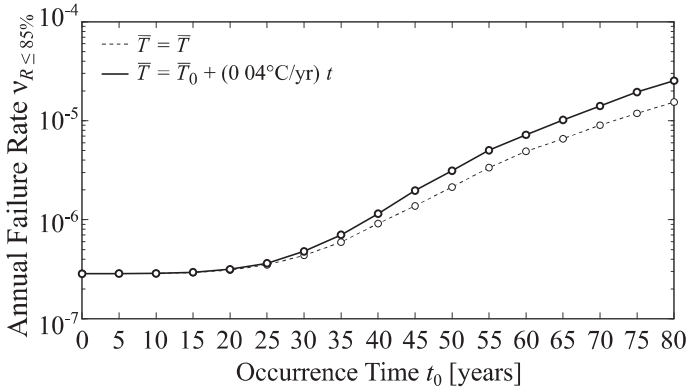

Figure 9. Lifetime annual failure rate with 85% resilience target with (continuous line) and without (dashed line) climate change.

5 CONCLUSIONS

Depending on environmental aggressiveness, RC bridges may suffer significant reduction of seismic capacity over time leading to intensify the potential impact of severe earthquakes at the network level. These effects can be exacerbated by climate change effects. A probabilistic framework for lifetime seismic risk assessment of aging bridge networks has been proposed based on the definition of a quantitative measure of system resilience. The impact of climate change on seismic risk of aging has been taken into account considering scenarios of seasonal variations and increasing average temperatures. The progressively increasing seismic vulnerability of exposed bridges induced by corrosion and rising temperatures can severely affect the annual rate of failing to meet suitable resilience target.

The proposed application emphasizes the importance of formulating appropriate lifetime performance indicators that would inform design, maintenance and retrofit policies supporting the decision making process for new and existing structures under climate change. Further research efforts should be devoted to the incorporation of additional climate change factors, such as the impact of gas emissions, on both the occurrence and rate of deterioration processes and other related hazards.

REFERENCES

Almusallam, A.A. 2001. Effect of degree of corrosion on the properties of reinforcing steel bars. *Construction and Building Materials*, 15, 361–368

Ang, A. H. S., & Tang, W. H. (2007). *Probability concepts in engineering: Emphasis on applications to civil and environmental engineering*, Hoboken, NJ, Wiley

Apostolopoulos, C.A., & Papadakis, V.G. 2008. Consequences of steel corrosion on the ductility properties of reinforcement bar. *Construction and Building Materials*, 22(12), 2316-2324.

Barani, S., Spallarossa, D., & Bazzurro, P. 2009. Disaggregation of probabilistic ground-motion hazard in Italy, *Bulletin of the Seismological Society of America*, 99(5), 2638-2661.

Baker J.W., 2009. *An introduction to probabilistic seismic hazard analysis (PSHA)*. White Paper, version 1.3.

Basoz, N., & Kiremidjian, A. S. 1998. *Evaluation of bridge damage data from the Loma Prieta and Northridge, California earthquakes*. Technical Report, MCEER-98-0004.

Bastidas-Arteaga E., Schoefs F., Stewart M.G., & Wang X. 2013. Influence of global warming on durability of corroding RC structures: a probabilistic approach, *Engineering Structures*, 51, 259-266.

Bertolini L., Elsener B., Pedeferri P., & Polder R. 2004. *Corrosion of steel in concrete*. Weinheim, Germany: Wiley-VCH.

Bindi, D., Pacor, F., Luzi, L., Puglia, R., Massa, M., Ameri, G., & Paolucci, R., 2011. Ground motion prediction equations derived from the Italian strong motion database. *Bulletin of Earthquake Engineering*, 9(6), 1899-1920.

Biondini F., Bontempi F., Frangopol D.M., & Malerba P.G. 2004. Cellular automata approach to durability analysis of concrete structures in aggressive environments. *Journal of Structural Engineering*, ASCE, 130(11), 1724 1737.

Biondini F., Frangopol D.M., & Malerba P.G. 2006. Time-variant performance of the Certosa cable-stayed bridge. *Structural Engineering International*, IABSE, 16(3), 235-244.

Biondini F., Camnasio E., & Titi A. 2015. Seismic resilience of concrete structures under corrosion, *Earthquake Engineering & Structural Dynamics*, 44(14), 2445-2466.

Biondini, F., & Vergani, M. 2015. Deteriorating beam finite element for nonlinear analysis of concrete structures under corrosion, *Structure and Infrastructure Engineering*, 11(4), 519-532.

Bouassida, Y., Bouchon, E., Crespo, P., Croce, P., Davaine, L., Denton, S., Feldmann, M., Frank, R., Hanswille, G., Hensen, W., Kolias, B., Malakatas, N., Mancini, G., Ortega, M., Raoul, J., Sedlacek, G., & Tsionis, G. 2012. *Bridge design to Eurocodes. Worked examples*. JRC Scientific and Technical Reports, EUR 25193 EN-2012.

Bruneau, M, Chang, S.E., Eguchi, R.T., Lee, G.C., O'Rourke, T.D., Reinhorn, A.M., Shinozuka, M., Tierney, K., Wallace, W.A., & von Winterfeldt, D. 2003. A framework to quantitatively assess and enhance the seismic resilience of communities. *Earthquake Spectra*, 19(4), 733-752.

Capacci, L., & Biondini, F. 2018. Life-cycle seismic resilience of aging bridges and road networks considering bridge capacity correlation. *9th International Conference on Bridge Maintenance, Safety and Management*, Melbourne, Australia, July 9-13, 2018. In: *Maintenance, Safety, Risk, Management and Life-Cycle Performance of Bridges.* N. Powers, D.M. Frangopol, R. Al-Mahaidi, C. Caprani (Eds.), CRC Press/ Balkema, Taylor & Francis Group, London, UK.

Capacci, L., & Biondini, F. 2019. Seismic resilience of bridges and road networks under climate change. *2019 IABSE Congress New York City, The Evolving Metropoli*s. September 4-6, 2019, New York, NY, USA.

Capacci L., & Biondini F. 2020. Probabilistic life-cycle seismic resilience assessment of aging bridge networks considering infrastructure upgrading. *Structure and Infrastructure Engineering*, Online First Publication, DOI: 10.1080/15732479.2020.1716258

Capacci L., Biondini F., & Titi A. 2020. Lifetime seismic resilience of aging bridges and road networks. *Structure and Infrastructure Engineering*, 16(2), 266-286.

Decò, A., Bocchini, P., & Frangopol, D.M. 2013. A probabilistic approach for the prediction of seismic resilience of bridges. *Earthquake Engineering & Structural Dynamics*. 42(10), 1469-1487.

DuraCrete. 2000. *Probabilistic calculations. DuraCrete—probabilistic performance-based durability design of concrete structures*. EU—brite EuRam III. Contract BRPR-CT95-0132. Project BE95-1347/R12-13. May 2000. p. 41.

fib. 2006. *Model Code for Service Life Design*. fib, Bulletin 34, Lausanne, Switzerland.

Gonzalez, J.A., Andrade, C., Alonso, C., & Feliu, S. 1995. Comparison of rates of general corrosion and maximum pitting penetration on concrete embedded steel reinforcement. *Cement and Concrete Research*, 25, 257-264.

IPCC. 2014. *Climate change 2014: Synthesis report. Contribution of Working Groups I, II and III to fifth assessment report*. Core Writing Team, R.K. Pachauri, L.A. Meyer (Eds.). Intergovernmental Panel on Climate Change, Geneva, Switzerland.

Jayaram, N., & Baker, J.W. 2010. Efficient sampling and data reduction techniques for probabilistic seismic lifeline risk assessment. *Earthquake Engineering & Structural Dynamics*, 39, 1109-1131.

Kumar, R., Gardoni, P., & Sanchez-Silva, M. 2009. Effect of cumulative seismic damage and corrosion on the life-cycle cost of reinforced concrete bridges. *Earthquake Engineering & Structural Dynamics*, 38, 887-905.

Lallemant, D., Kiremidjian, A., & Burton, H. 2015. Statistical procedures for developing earthquake damage fragility curves. *Earthquake Engineering & Structural Dynamics*, 44(9), 1373-1389.

Marí, A., & Bairán, J.M. 2008. Evaluation of the response of concrete structures along their service life by nonlinear evolutive analysis methods. *First International Symposium on Life-Cycle Civil Engineering* (IALCCE'08), Varenna, Lake Como, Italy, June 11-14. In: *Life-Cycle Civil Engineering.* F. Biondini, D.M. Frangopol (Eds.), CRC Press/Balkema, Taylor & Francis Group, London, UK.

McGuire R.K. 2007. *Seismic Hazard and Risk Analysis*, EERI.

Mondoro, A., Frangopol, D.M., & Liu, L. 2017. Bridge adaptation and management under climate change uncertainties: a review. *Natural Hazards Review*, 19(1), 04017023.

Nasr, A., Björnsson, I., Honfi, D., Larsson Ivanov, O., Johansson, J., & Kjellstrom, E. 2019. A review of the potential impacts of climate change on the safety and performance of bridges. *Sustainable and Resilient Infrastructure*, Online First Publication, DOI: 10.1080/23789689.2019.1593003.

Stewart M. G., Wang X., & Nguyen M. 2011. Climate change impact and risks of concrete infrastructure deterioration. *Engineering Structures*, 33, 1326-1337.

Titi, A., & Biondini, F. 2016. On the accuracy of diffusion models for life-cycle assessment of concrete structures. *Structure and Infrastructure Engineering*, 12(9), 1202-1215.

Val D.V., & Melchers R.E. 1997. Reliability of deteriorating RC slab bridges. *Journal of Structural Engineering*, 123(12), 1638-1644.